obtained from Invitrogen (Carlsbad, CA). The pairs of each small interfering RNA (siRNA) and novel RNAi reagent, targeting luciferase mRNA, and human RPN2 mRNA (Supplementary Table 1, 2) were purchased from Bonac (Kurume, Japan). Allstars Negative Control siRNA was obtained from Qiagen (Hilden, Germany).

Preparation of novel RNAi agents. The preparation of proline diamide amidite and the novel RNAi agents has been previously described[9]. Novel RNAi agents are prepared as single-stranded RNA that self-anneals into a unique structure containing a double-stranded RNA with an unpaired site bound at the right and left ends by an oligonucleotide loop or by a non-nucleotide molecule (a proline derivative). Fig. 1 shows the schematic model of human RPN2, which was selected as a representative RNAi target.

RNA stability. To estimate the resistance to nucleases, 40 μl (2 μmol/l) of siRNA, nkRNA and PnkRNA directed against human RPN2 were incubated at 37°C with 1 μl of RNase Cocktail Enzyme Mix (Ambion, Foster City, CA) (RNase A 500 U/ml, RNase T1 20,000 U/ml). After the specified times, the ribonuclease reaction was stopped, and 2 μl of each sample was run on 3% agarose gel.

Cell line. A549-luc-C8 cells, a luciferase-expressing cell line derived from A549 human lung adenocarcinoma cells by stable transfection of the North American Firefly Luciferase gene expressed from the CMV promoter, were purchased from Xenogen. The human lung adenocarcinoma cell line PC14 was obtained from RIKEN BioResource Center (Tokyo, Japan). These cells were cultured in RPMI-1640 containing 10% heat-inactivated FBS and an antibiotic-antimycotic at 37°C in 5% CO_2.

RNA extraction. Total RNA was extracted from cultured cells or mice lungs using QIAzol and miRNeasy Mini Kit (Qiagen) according to the manufacturer's protocol. The purity and concentration of all RNA samples were quantified using NanoDrop ND-1000 (Thermo Scientific, San Jose, CA). For RPN2 mRNA analysis of mice lungs, the animals were sacrificed 24 h after the inhaled administration of each RNAi agent.

Quantitative Real-time PCR (qRT-PCR). The reverse transcription reaction was performed with a High-Capacity cDNA Reverse Transcription Kit (Applied Biosystems, Foster City, CA) using a random hexamer primer. The synthesised cDNAs were quantified by SYBR Green I qRT-PCR. Quantitative real-time reverse transcription-PCR (qRT-PCR) analysis was conducted using primers for human RPN2 (forward:5′-CTTCCAGAGCCACTGTCCTC-3′; reverse: 5′-CCGGTTGTC-ACCTTCAACTT-3′). β-Actin (forward:5′-ATTGCCGACAGGATGCAGA-3′; reverse:5′-GAGTACTTGCGCTCAGGAGGA-3′) was used for normalisation. The relative amounts of RPN2 were measured using the 2(-Delta Delta C(T)) method. The reactions were performed with the ABI Prism 7300 Sequence Detection System (Applied Biosystems) at 95°C/10 min, followed by 40 cycles at 95°C/15 s and 60°C/30 s. All qRT-PCR reactions were performed in triplicate.

Transient transfection assays. A549-luc-C8 cells were plated on six-well plates at a density of 2×10^5 cells/well and grown overnight until 50–80% confluence was achieved to obtain maximum transfection efficiency. The cells were transfected with validated siRNA, the novel RNAi agents (PnkRNA, nkRNA) for RPN2, or Allstars Negative Control siRNA (Qiagen) at a final concentration of 25 nmol/l using the DharmaFECT 1 reagent (Thermo Scientific), according to the manufacturer's protocol. In the cDNA rescue experiment, an RPN2 Human cDNA ORF clone (Origene Technologies, Rockville, MD) or pEGFP-N1 (Clontech Laboratories, Mountain View, CA) was combined with each siRNA using DharmaFECT Duo (Thermo Scientific), according to the manufacturer's protocol. RPN2-siRNA targeting site is located 906 nt downstream of the ATG start codon of human RPN2 cDNA sequence on human RPN2 expression vector.

Cell Proliferation Assay (MTS assay). A Cell Counting Kit-8 (CCK-8) (Dojindo Laboratories, Kumamoto, Japan) was used in the cell proliferation assay. Five thousand cells per well were seeded in 96-well plates. The following day, the cells were replenished with fresh medium containing 25 nmol/l of each RNAi agent. After four days of culture, a plate was assayed by adding 10 μl of CCK-8 solution to each well, and the plate was further incubated for 4 h at 37°C. The absorbance at 450 nm was measured using Envision (PerkinElmer, Norwalk, CT).

RNAi therapeutic agent labelling with pHrodo™ Red succinimidyl ester and endocytosis assay. The fluorescence of the pHrodo™ Red dye increases as the pH decreases from neutral to acidic, making it an ideal tool to study endocytosis[25]. The amine-reactive forms of pHrodo™ Red succinimidyl ester were used for labelling the RNAi therapeutic agents. After being labeled according to the manufacturer's protocol, the oligonucleotides were purified by reverse-phase HPLC. A549-luc-C8 cells or PC14 cells were transfected with the labeled siRNAs or PnkRNAs. Each labeled oligonucleotide was transfected with or without DharmaFECT 1 reagent. Then, the plates were incubated at 37°C for 3 hours to allow endocytosis to run to completion. Hoechst 33342 was used as a DNA counter-stain (cyan). Microscopic analysis was performed with a FLUOVIEW FV10i confocal microscope.

***In vivo* imaging of RNAi therapeutic agents in mice with lung cancer.** Animal experiments were performed in compliance with the guidelines of the Institute for Laboratory Animal Research, National Cancer Center Research Institute. These studies were approved by the National Cancer Center Research Institute. Six- to seven-week-old male C.B-17/Icr-scid/scidJcl mice (CLEA Japan, Shizuoka, Japan) were used in the experiments. The animals were housed in a 12 h light/12 h dark cycle and provided with an autoclaved rodent diet and water *ad libitum*. The mice were injected intravenously with 2×10^6 A549-luc-C8 cells suspended in 0.25 ml of sterile Dulbecco's PBS via the tail vein (day 0). For *in vivo* imaging, the mice were administered 150 mg/kg D-luciferin (Promega, Madison, WI) by intraperitoneal injection. Ten minutes later, photons from the whole bodies of the animals were counted by measuring bioluminescence with an IVIS imaging system (Xenogen, Alameda, CA), according to the manufacturer's instructions. The data were analysed using LIVINGIMAGE 4.2 software (Xenogen). The development of lung cancer was monitored twice a week *in vivo* by bioluminescent imaging. Four weeks after tumor injection (day 28), the bioluminescence from the implanted cancer cells was measured, and the mice were divided into four treatment groups (single administration study, mice per group; n = 4) or two groups (repeated administration study, mice per group; n = 12) with equivalent levels of bioluminescence. In the single administration study, the individual mice were administered 15 μg of each RNAi agent with *In vivo*-jetPEI™ (Polyplus Transfection Inc, New York, NY) (resulting in a calculated 1 : 6 charge ratio of nucleic acid backbone phosphates to cationic lipid nitrogen atoms) in a volume of 25 μl on day 28 using an endotracheally inserted MicroSprayer™ aerosoliser (IA-1C; Penn-Century) and a high-pressure syringe (FMJ-250; Penn-Century, Philadelphia, PA)[26]. Data are from a representative experiment of three independent experiments. In the repeated administration study, the treatment—15 μg of each naked RNAi agent inhaled by using a MicroSprayer™ aerosoliser—was performed on days 28, 35, and 42 (once a week for 3 weeks, three treatments total). To control for mouse-to-mouse variability, the bioluminescence ratio for each mouse was normalised by dividing by each day of the post-treatment/pre-treatment (day28) ratio of luciferase intensity for that mouse. For *in vivo* knockdown analysis, animals were sacrificed 24 h after each RNAi application, and lungs were removed and processed for histology or knockdown determination by qRT-PCR (SYBR Green).

Lung histological findings. Lung tissues were fixed in 10% neutral buffered formalin, paraffin-processed, and sectioned at 5 μm. Formalin-fixed and paraffin-embedded slides were stained with haematoxylin and eosin (H&E) or used for immunohistochemical (IHC) staining. With regard to the histologic estimation of tumor burden, the freeware *Image J* (National Institutes of Health, Bethesda, Maryland, USA) was used. Upon the IHC staining, antigen retrieval was performed by autoclave in a 10 mmol/l sodium citrate buffer (pH 6.0), and the endogenous peroxidase activity was blocked with the Immuno Pure Peroxidase Suppressor (Pierce, Chester, UK). The slides were incubated with RPN2 (A-1, Santa Cruz Biotechnology, Santa Cruz, CA) or Ki-67 (M7240, Dako Cytomation, Copenhagen, Denmark) primary antibody at 4°C overnight. The next day, after washing, the samples were incubated with mouse peroxidase-conjugated anti-mouse IgG (ImmPRESS Reagent; Vector Labs, Burlingame, CA) for 1 h. The immunoreactions were visualised with diaminobenzidine, and the sections were counterstained with haematoxylin.

Immunofluorescence staining. To estimate the inhaled distribution of RNAi agents, 15 μg of Allstars NegativesiRNA Alexia Fluor 647 (Qiagen) with *In vivo*-jetPEI™ was aerosolised by means of a MicroSprayer™, and the lungs were harvested 6 h after application, processed for paraffin sectioning, and analysed by confocal microscopy. DAPI staining was carried out immediately before imaging. Imaging for the cyan (DAPI) and magenta (fluorescently labeled siRNA) channels was performed in sequential mode using the appropriate excitation and emission settings. Microscopic analysis was performed with a FLUOVIEW FV10i confocal microscope (OLYMPUS, Tokyo, Japan).

Statistical analysis. All experiments were repeated at least three times, and the results are expressed as the means ± SE. The statistical analyses were conducted using the Bonferroni multiple-comparison test. These analyses were performed with the Expert StatView analysis software (version 4; SAS Institute, Cary, NC). $P < 0.05$ was considered to be statistically significant.

1. Matranga, C., Tomari, Y., Shin, C., Bartel, D. P. & Zamore, P. D. Passenger-strand cleavage facilitates assembly of siRNA into Ago2-containing RNAi enzyme complexes. *Cell* **123**, 607–620 (2005).
2. Davidson, B. L. & McCray, P. B., Jr. Current prospects for RNA interference-based therapies. *Nat Rev Genet* **12**, 329–340 (2011).
3. Takeshita, F. & Ochiya, T. Therapeutic potential of RNA interference against cancer. *Cancer Sci* **97**, 689–696 (2006).
4. Kim, D. H. & Rossi, J. J. Strategies for silencing human disease using RNA interference. *Nat Rev Genet* **8**, 173–184 (2007).
5. Pecot, C. V., Calin, G. A., Coleman, R. L., Lopez-Berestein, G. & Sood, A. K. RNA interference in the clinic: challenges and future directions. *Nat Rev Cancer* **11**, 59–67 (2011).
6. Chernolovskaya, E. L. & Zenkova, M. A. Chemical modification of siRNA. *Curr Opin Mol Ther* **12**, 158–167 (2010).
7. Lares, M. R., Rossi, J. J. & Ouellet, D. L. RNAi and small interfering RNAs in human disease therapeutic applications. *Trends Biotechnol* **28**, 570–579 (2010).

8. Zhou, J., Bobbin, M. L., Burnett, J. C. & Rossi, J. J. Current progress of RNA aptamer-based therapeutics. *Front Genet* **3**, 234 (2012).
9. Hamasaki, T. *et al.* Efficacy of a novel class of RNA interference therapeutic agents. *PLoS One* **7**, e42655 (2012).
10. Molina, J. R., Yang, P., Cassivi, S. D., Schild, S. E. & Adjei, A. A. Non-small cell lung cancer: epidemiology, risk factors, treatment, and survivorship. *Mayo Clin Proc* **83**, 584–594 (2008).
11. Ramalingam, S. S., Owonikoko, T. K. & Khuri, F. R. Lung cancer: New biological insights and recent therapeutic advances. *CA Cancer J Clin* **61**, 91–112 (2011).
12. Herbst, R. S., Heymach, J. V. & Lippman, S. M. Lung cancer. *N Engl J Med* **359**, 1367–1380 (2008).
13. Pao, W. & Girard, N. New driver mutations in non-small-cell lung cancer. *Lancet Oncol* **12**, 175–180 (2011).
14. Agu, R. U., Ugwoke, M. I., Armand, M., Kinget, R. & Verbeke, N. The lung as a route for systemic delivery of therapeutic proteins and peptides. *Respir Res* **2**, 198–209 (2001).
15. Lam, J. K., Liang, W. & Chan, H. K. Pulmonary delivery of therapeutic siRNA. *Adv Drug Deliv Rev* **64**, 1–15 (2012).
16. Morin, A., Gallou-Kabani, C., Mathieu, J. R. & Cabon, F. Systemic delivery and quantification of unformulated interfering RNAs in vivo. *Curr Top Med Chem* **9**, 1117–1129 (2009).
17. Heidel, J. D., Hu, S., Liu, X. F., Triche, T. J. & Davis, M. E. Lack of interferon response in animals to naked siRNAs. *Nat Biotechnol* **22**, 1579–1582 (2004).
18. Burnett, J. C. & Rossi, J. J. RNA-based therapeutics: current progress and future prospects. *Chem Biol* **19**, 60–71 (2012).
19. Schlee, M., Hornung, V. & Hartmann, G. siRNA and isRNA: two edges of one sword. *Mol Ther* **14**, 463–470 (2006).
20. Petrocca, F. & Lieberman, J. Promise and challenge of RNA interference-based therapy for cancer. *J Clin Oncol* **29**, 747–754 (2011).
21. Honma, K. *et al.* RPN2 gene confers docetaxel resistance in breast cancer. *Nat Med* **14**, 939–948 (2008).
22. Zhu, J., He, J., Liu, Y., Simeone, D. M. & Lubman, D. M. Identification of glycoprotein markers for pancreatic cancer CD24+CD44+ stem-like cells using nano-LC-MS/MS and tissue microarray. *J Proteome Res* **11**, 2272–2281 (2012).
23. Kurashige, J. *et al.* RPN2 expression predicts response to docetaxel in oesophageal squamous cell carcinoma. *Br J Cancer* **107**, 1233–1238 (2012).
24. Takahashi, R. *et al.* Ribophorin II regulates breast tumor initiation and metastasis through the functional suppression of GSK3β. *Sci. Rep.* **3**, 2474; doi:10.1038/srep02474 (2013).
25. Han, J. & Burgess, K. Fluorescent indicators for intracellular pH. *Chem Rev* **110**, 2709–2728 (2010).
26. Bivas-Benita, M., Zwier, R., Junginger, H. E. & Borchard, G. Non-invasive pulmonary aerosol delivery in mice by the endotracheal route. *Eur J Pharm Biopharm* **61**, 214–218 (2005).

Acknowledgments

This work was supported in part by a grant-in-aid for the Third-Term Comprehensive 10-Year Strategy for Cancer Control of Japan; Project for Development of Innovative Research on Cancer Therapeutics (P-Direct); Scientific Research on Priority Areas Cancer, Scientific Research on Innovative Areas ("functional machinery for non-coding RNAs") from the Japanese Ministry of Education, Culture, Sports, Science, and Technology; the National Cancer Center Research and Development Fund (23-A-2, 23-A-7, 23-C-6,); the Program for Promotion of Fundamental Studies in Health Sciences of the National Institute of Biomedical Innovation (NiBio), the Project for Development of Innovative Research on Cancer Therapeutics; and the Japan Society for the Promotion of Science (JSPS) through the "Funding Program for World-Leading Innovative R&D on Science and Technology (FIRST Program)" initiated by the Council for Science and Technology Policy (CSTP). We thank Ayako Inoue and Maki Abe for her excellent technical assistance.

Author contributions

T. Ochiya and K.K. conceived the idea and coordinated the project. Y.F. performed a significant amount of the experimental work. T. Ochiya, Y.F., F.T., T.M. and T. Ohgi wrote the manuscript and prepared the figures and tables. In vivo experiments were carried out by Y.F. and F.T.

Additional information

Supplementary information accompanies this paper at http://www.nature.com/scientificreports

Competing financial interests: The authors declare no competing financial interests.

How to cite this article: Fujita, Y. *et al.* A novel platform to enable inhaled naked RNAi medicine for lung cancer. *Sci. Rep.* **3**, 3325; DOI:10.1038/srep03325 (2013).

Pathology International

Pathology International 2013; **63**: 408–414 doi:10.1111/pin.12086

Original Article

Parp-1 deficiency in ES cells promotes invasive and metastatic lesions accompanying induction of trophoblast giant cells during tumorigenesis in uterine environment

Tadashige Nozaki,[1,4] Hiroaki Fujimori,[1,2] Junhui Wang,[2] Hiroshi Suzuki,[5] Hiroshi Imai,[6] Masatoshi Watanabe,[7] Kiyoshi Ohura[4] and Mitsuko Masutani[1,2,3]

Divisions of [1]Biochemistry and [2]Genome Stability Research, and [3]ADP-Ribosylation in Oncology Project, National Cancer Center Research Institute, Tokyo, [4]Department of Pharmacology, Osaka Dental University, Osaka, [5]Research Unit for Functional Genomics, National Research Center for Protozoan Diseases, Obihiro University of Agriculture and Veterinary Medicine, Obihiro, [6]Pathology Division, Mie University Hospital, Mie, and [7]Laboratory for Medical Engineering, Division of Materials Science and Chemical Engineering, Graduate School of Engineering, Yokohama National University, Yokohama, Japan

Embryonic stem (ES) cells deficient in poly(ADP-ribose) polymerase-1 (Parp-1) develop into teratocarcinomas with the appearance of trophoblast giant cells (TGCs) when injected subcutaneously into nude mice. Because the uterus is one of the original organs in which germ cell tumors develop with induction of trophoblast lineage, here we investigated whether *Parp-1* deficiency in ES cells affects teratocarcinoma formation processes by grafting ES cells into the horns of uteri. Teratocarcinomas developed from both wild-type (*Parp-1*$^{+/+}$) and *Parp-1*$^{-/-}$ ES cells. The weights of the tumors derived from *Parp-1*$^{-/-}$ ES cells were lower than those of the tumors derived from *Parp-1*$^{+/+}$ ES cells ($P < 0.05$). The *Parp-1*$^{-/-}$ tumors showed the appearance of TGCs. Notably, organ metastasis to the lung and liver was observed for the *Parp-1*$^{-/-}$ tumors, but not for the *Parp-1*$^{+/+}$ tumors ($P < 0.05$). Invasions were more frequently observed with the *Parp-1*$^{-/-}$ tumors compared with the *Parp-1*$^{+/+}$ tumors ($P < 0.05$). Since TGCs are known to have invasive properties, the appearance of TGCs may have supported the metastatic process. The present findings suggest that loss of *Parp-1* during teratocarcinoma formation might augment invasive and metastatic properties of the tumors in the uterine environment.

Key words: ES cell, metastasis, Parp-1, teratocarcinoma, trophoblast giant cell, uterus

Correspondence: Mitsuko Masutani, PhD, Division of Genome Stability Research, National Cancer Center Research Institute, 1-1 Tsukiji 5-chome, Chuo-ku, Tokyo 104-0045, Japan. Email: mmasutan@ncc.go.jp

Received 13 April 2013. Accepted for publication 6 July 2013.

Poly(ADP-ribosylation) is catalyzed by poly(ADP-ribose) polymerase-1 (Parp-1) and other PARP family proteins.[1–4] Parp-1 is activated by DNA strand breaks and is involved in DNA damage repair.[5,6] It is also activated by nucleosomes or histones and participates in the regulation of transcription, chromatin remodeling, and differentiation.[7–9] Subcutaneous injection of *Parp-1*$^{-/-}$ embryonic stem (ES) cells into nude mice leads to the formation of *Parp-1*$^{-/-}$ ES cell-derived tumors, which are characterized by extensive blood pools and the appearance of trophoblast giant cells (TGCs) and spongiotrophoblasts belonging to the trophoblast lineage.[10] During culture of *Parp-1*$^{-/-}$ ES cells in the presence of leukemia inhibitory factor (LIF), the appearance of TGCs was observed at an increased frequency.[11] After LIF removal, the frequency of the TGC population increased within several days.[11] Induction of trophoblast marker genes, including the *caudal-related homeobox 2* (*cdx2*) and *proliferin* (*plf*) genes, was also observed in *Parp-1*$^{-/-}$ ES cells after removal of LIF.[12] Therefore, loss of *Parp-1* is suggested to induce trophoblast differentiation of mouse ES cells not only during teratocarcinoma formation but also during culture.[11,13] The tumor formation process and induction of trophoblast lineage differentiation are supposed to be affected by the tissue environment in the uterus. Trophoblast induction should affect the biological properties of tumors, including their growth, invasiveness, and metastasis. During subcutaneous teratocarcinoma formation, no difference in tumor growth was observed between *Parp-1*$^{-/-}$ and *Parp-1*$^{+/+}$ ES cells.[1] The uterus is one of the original organs in which germ cell tumors develop and trophoblast lineage cells reside and differentiate.[14] It is reported that when ES cells are injected to non-pregnant uteri, teratocarcinoma is developed.[14] Therefore in

the present study, we examined whether the deficiency of *Parp-1* in ES cells injected into the uterus affects the teratocarcinoma formation and tumor properties, including the induction of trophoblast lineage differentiation.

MATERIALS AND METHODS

Cells and culture conditions

Parp-1$^{+/+}$ ES cells (J1) and *Parp-1*$^{-/-}$ ES cells were cultured in Dulbecco's modified Eagle's medium (Life Technologies Corp., Carlsbad, CA) supplemented with 20% fetal bovine serum, non-essential amino acids (Life Technologies Corp.), 55 μM β-mercaptoethanol, 0.3 mM each of adenosine, guanosine, and thymidine, 0.1 mM uridine, and 1×10^3 U/mL mouse LIF (Chemicon International Inc., Temecula, CA) on gelatin-coated dishes (Asahi Glass Co. Ltd, Tokyo, Japan). The *Parp-1*$^{-/-}$ ES cell clone analyzed was clone 210-58, as described previously.[1]

Injection of ES cells into the horn of the uterus of nude mice

Embryonic stem cells were grown approximately to 50% confluence in the absence of an STO cell feeder layer on 100-mm culture plates, and then harvested with a cell scraper and resuspended in phosphate-buffered saline (PBS). Aliquots of 2×10^6 ES cells of each *Parp-1* genotype were injected through the back into the horn of the uterus of ten 8-week-old female BALB/c nu/nu mice (CLEA Japan Inc., Tokyo, Japan). Subsequently, the conditions of the whole body and the transplant parts of mice were observed every day. The mice were sacrificed when demonstrating over 20% decrease in body weight excluding total tumor weight and/or when symptoms of poor physical condition, such as decrease in locomotor activity, were found. Volume of tumors was not considered important in this regard, since changes in tumor volume was a key item for evaluation of the effects of genotypes. Four weeks after the ES cell injection, the mice were euthanized and the status of uterus was evaluated at each group by monitoring the weight of tumors immediately after resection. Visible macroscopic metastasis in various organs were also determined at euthanasia.

Ethics statement

All animal experiments were approved by the Institutional Animal Experiment Committee of the National Cancer Center Research Institute. All animal works were conducted according to relevant national and international guidelines for animal welfare.

Preparation of a polyclonal antibody against mouse placental lactogen I

A synthetic peptide corresponding to the C-terminal 16-amino acid sequence of mouse placental lactogen I (M35662) was generated by Sawady Technology Co. Ltd. (Tokyo, Japan). An antibody against the peptide was generated in rabbits and purified using CNBr-activated Sepharose 4B coupled with the peptide by the same company. The antibody was confirmed to detect mouse placental lactogen I as a single band of the correct size (data not shown).

Histopathological analysis of tumors

After resection, excised tissues were fixed in neutralized 10% formalin solution for approximately 12 h and then embedded in paraffin blocks using standard procedures.[10] Slice sections (5 μm) were stained with hematoxylin and eosin (H&E) and observed under an optical microscope equipped with a charge coupled device (CCD) camera system (Olympus, Tokyo, Japan) to evaluate pathological findings such as local invasion and microscopic metastasis.

Immunohistochemical staining

Tissue sections (5 μm) were mounted on poly-L-lysine-coated slides, deparaffinized with xylene, and rehydrated in a graded alcohol series. After inactivation of endogenous peroxidase with 0.3% hydrogen peroxide in methanol for 30 min and blocking with PBS(–) containing 2% normal goat serum for 30 min, the sections were incubated with the rabbit anti-mouse placental lactogen I polyclonal antibody after 240-fold dilution (10 μg/mL) in PBS(–) containing 2% goat serum for 12 h at 4°C in a humidified chamber. The prolactin antibody (Biogenesis, Bournemouth, U.K.) after 200-fold dilution was also used as described.[10] The sections were then incubated with biotinylated goat anti-rabbit IgG (Vector Laboratories Inc., Burlingame, CA) diluted 200-fold in PBS containing 2% goat serum as the secondary antibody. Bound antibodies were detected by staining with a Vectastain ABC Kit (Vector Laboratories Inc.). The sections were counterstained with hematoxylin. As a negative control, duplicate sections were immunostained without exposure to the primary antibody.

Statistical analyses

Differences in the tumor weights were evaluated statistically by the Kruskal–Wallis test and the Mann–Whitney U test

Table 1 Microscopic findings

Group	Genotype	Tumor in uterus	TGCs	Dissemination	Invasion	Organ metastasis
1	+/+	+	None	Liver, Spleen*	None	None
	+/+	+	None	Pancreas, Intestine*	None	None
	+/+	+	None	None	None	None
	+/+	+	None	Liver*	None	None
	+/+	+	None	None	None	None
	+/+	+	None	None	None	None
	+/+	None	None	Pancreas, Spleen*, Muscle layers	Muscle layers	None
	+/+	None	None	None	None	None
	+/+	None	None	Spleen*	None	None
2	–/– (210-58)	+	+	Spleen*	None	Liver (central vein), Lung
	–/– (210-58)	+	+	Spleen*, Liver*, Lung*, Pancreas*, Abdominal vessel	Pancreas, Spleen, Liver, Lung, Abdominal vessel	Hepatic hillus, Lung
	–/– (210-58)	+	+	Pancreas	Pancreas	None
	–/– (210-58)	+	+	Pancreas, Abdominal muscle	Pancreas, Vessle in lung, Abdominal muscle	Vessle in lung
	–/– (210-58)	+	None	None	None	None
	–/– (210-58)	None	None	None	None	None
	–/– (210-58)	+	None	Liver*	None	Dilated lymphoducts
	–/– (210-58)	+	+	Liver*, Abdominal muscle	Abdominal muscle	None
	–/– (210-58)	None	None	None	None	None
	–/– (210-58)	None	None	None	None	None

*, Tumors in capsule.

using IBM SPSS software (IBM Japan Co. Ltd, Tokyo, Japan). The frequencies of invasion and metastasis were evaluated by the χ^2-test using the IBM SPSS software. Values of $P < 0.05$ were considered to indicate statistical significance.

RESULTS

Tumor formation in the uterus of nude mice

Distinct tumors developed to touchable sizes on the back at 4 weeks after the injection. The tumors derived from both genotypes were covered by a capsule and developed in either the fallopian tubules or the serosa of the ovary and uterus. The frequencies of tumor formation in the uterus for the *Parp-1*$^{+/+}$ and *Parp-1*$^{-/-}$ ES cells were 6/9 (one mouse died by accident) and 7/10, respectively. The mean tumor sizes for *Parp-1*$^{-/-}$ cells were smaller than for *Parp-1*$^{+/+}$ cells (6.1 ± 1.3 g and 1.9 ± 0.7 g, respectively, $P < 0.05$). Detailed comparisons of the tissues and cell types present in the tumors are summarized in Table 1. All of the developed tumors for the two genotypes were composed of both undifferentiated tissues and differentiated germinal components, such as ectodermal, mesodermal, and endodermal tissue derivatives with various grades of differentiation. Neuroectodermal components were frequently observed in the tumors derived from both *Parp-1*$^{+/+}$ and *Parp-1*$^{-/-}$ ES cells.

Tumor invasion and metastatic lesions

The frequencies of invasion and metastatic lesions were compared between the tumors derived from *Parp-1*$^{+/+}$ and *Parp-1*$^{-/-}$ ES cells. In this study, metastatic lesions were analyzed by the two categories; peritoneal dissemination and other organ metastasis. When tumors were observed macroscopically on the surface of the organs, regardless of the invasion under capsule microscopically, they were categorized as dissemination. When tumors were observed in the parenchymal tissue and mesenchyme of the organs except for the uterus, they were categorized as organ metastasis.

As shown in Table 1, organ metastasis in the lung and/or liver (Fig. 1) were significantly higher ($P < 0.05$) with *Parp-1*$^{-/-}$ ES cells (4 of 7 animals that formed tumors in the uterus) than with *Parp-1*$^{+/+}$ ES cells (0 of 6 animals that formed tumors in the uterus).

Peritoneal dissemination of the tumors derived from both genotypes was frequently observed, on the surface of the spleen, pancreas, liver, and intestine. As shown in Table 1, invasions were significantly more common ($P < 0.05$) with *Parp-1*$^{-/-}$ ES cells (4 of 7 tumors in the uterus) than with *Parp-1*$^{+/+}$ cells (0 of 6 tumors in the uterus). In addition, invasion of the disseminated lesion to the abdominal muscles was frequently observed (Fig. 2). Disseminated lesions of *Parp-1*$^{-/-}$ ES cells demonstrate various tissue types as well as tumors of the uterus (Fig. 3a). These areas were composed of solid sheets of primitive embryonic cells with crowded, large, oval and basophilic nuclei, scant cytoplasm,

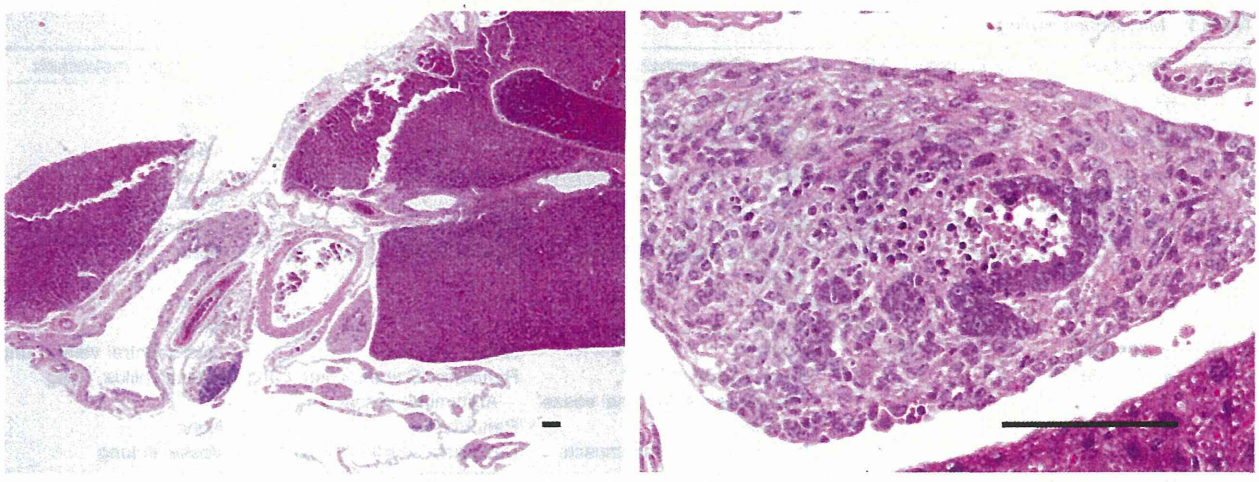

Figure 1 A metastatic lesion developed after grafting with *Parp-1*$^{-/-}$ embryonic stem (ES) cells. A metastastic lesion in the connective tissue around the portal vein of the liver in mice after grafting with *Parp-1*$^{-/-}$ ES cells (left panel). The right panel shows the magnified image. Bars indicate 100 μm.

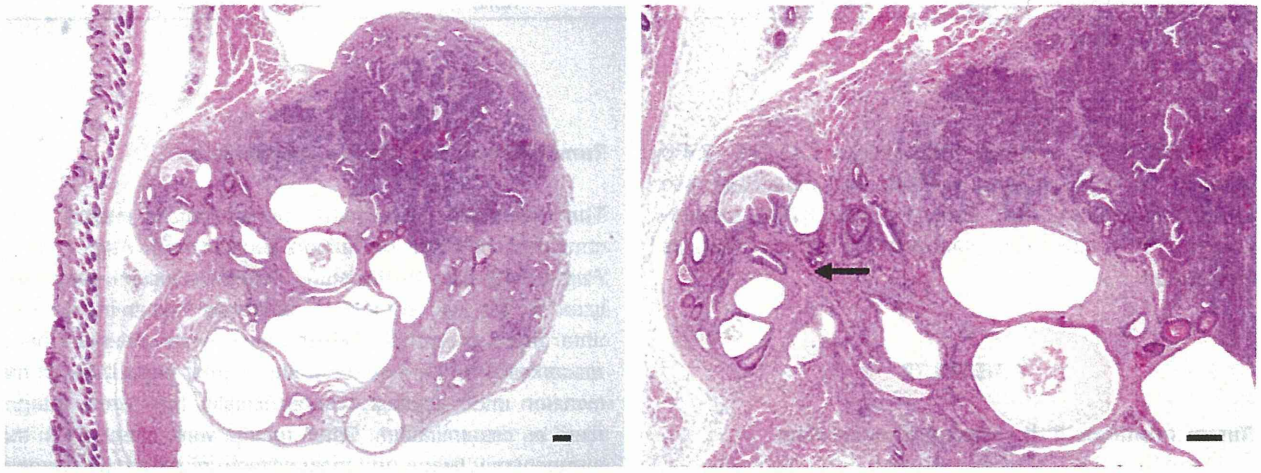

Figure 2 The lesions of invasion developed after grafting with *Parp-1*$^{-/-}$ embryonic stem (ES) cells (left panel). The arrow shows the invasion into the abdominal muscle. The right panel shows the magnified image. Bars indicate 100 μm.

and not distinct cytoplasm borders. The cells frequently formed rosettes within solid sheets (Fig. 3b).

In the three animals grafted with *Parp-1*$^{+/+}$ ES cells and two animals grafted with *Parp-1*$^{-/-}$ ES cells, tumors in the uterus were not observed but disseminated tumors were present.

Induction of TGCs and blood pools in tumors derived from *Parp-1*$^{-/-}$ ES cells

Overall, 6 of 7 tumors in the uterus (86%) derived from *Parp-1*$^{-/-}$ ES cells showed the development of extensive blood pools with giant cells (Fig. 4a). The components of the tumors were very similar among the two genotypes, except for the presence of extensive blood pools. The giant cells possessed megalonuclei and an eosinophilic cytoplasm, suggesting that they were similar to TGCs, as we previously observed in teratocarcinomas derived from *Parp-1*$^{-/-}$ ES cells after subcutaneous injection into nude mice.[10] To examine the properties of these giant cells, an anti-mouse placental lactogen I antibody was produced and checked for immunoreactivity against the TGCs of a mouse embryo placenta at E13.5, and positive staining was confirmed (Fig. 4b). Immunostaining of the tumors revealed that the cytoplasm of the giant cells showed positive staining for this anti-mouse placental lactogen I antibody (Fig. 4c). These giant cells are also positively stained with anti-prolactin antibody (Fig. 4d) as previously described for TGCs appeared in tumors

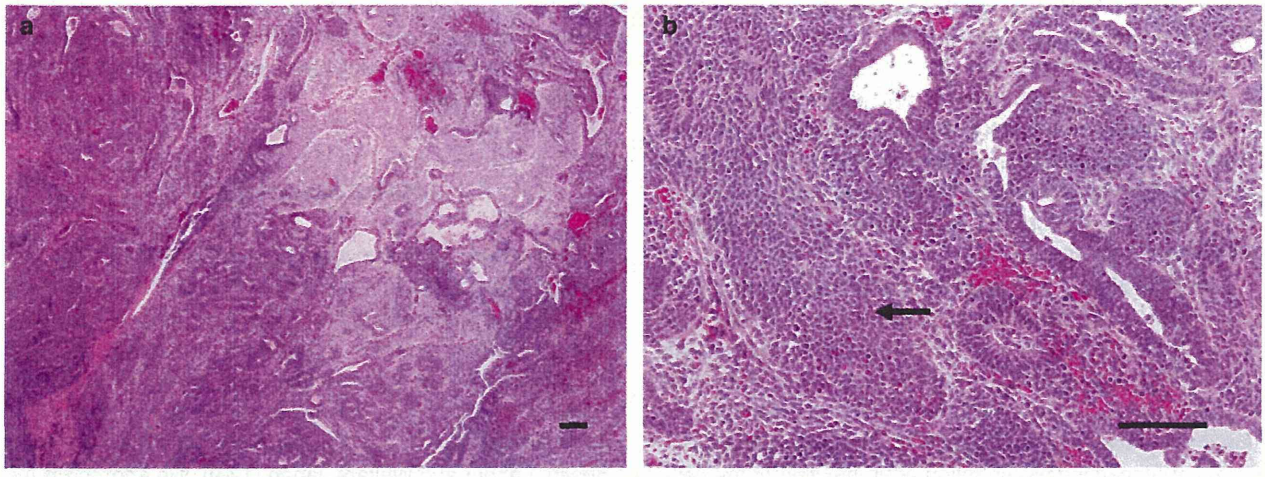

Figure 3 Disseminated lesions developed after grafting with *Parp-1*$^{-/-}$ embryonic stem (ES) cells. (**a**) The disseminated lesion demonstrates various tissue types such as glandular epithelium, but mainly neural tissues. (**b**) Primitive embryonic cells forming a rosette (arrow) and anaplastic cells were observed. Bars indicate 100 μm.

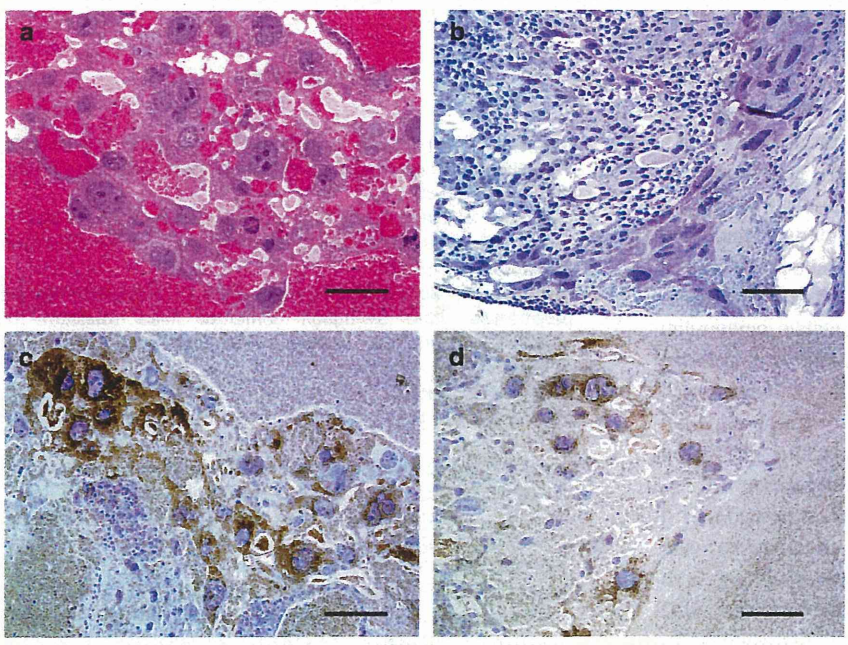

Figure 4 Trophoblast giant cells (TGCs) in the tumors developed after grafting with *Parp-1*$^{-/-}$ ES cells. (**a**) Hematoxylin and eosin staining of a tumor after grafting with *Parp-1*$^{-/-}$ embryonic stem (ES) cells. (**b**) Staining of an embryonic placenta at E13.5 with the anti-mouse placental lactogen I antibody. (**c**) Staining of a tumor with the anti-mouse placental lactogen I antibody. (**d**) Staining of a tumor with the anti-mouse prolactin antibody. The cytoplasmic regions containing the TGCs are positively stained with anti-placental lactogen and anti-prolactin antibodies. Bars indicate 100 μm.

derived from *Parp-1*$^{-/-}$ ES cells after subcutaneous injection.[10] These data support the notion that the developed giant cells in the teratocarcinomas derived from *Parp-1*$^{-/-}$ ES cells were TGCs.

DISCUSSION

Here we investigated whether uterine environment affects tumorigenesis from wild-type and *Parp-1* deficient ES cells compared to subcutaneous environment. The difference we observed between the subcutaneous and uterine environment were the tumor size and the frequencies of metastatic and invasive lesions. *Parp-1* deficiency in ES cells attenuated the growth of teratocarcinomas formed in the fallopian tubules and capsule of the ovary and uterus. Exposure of the grafted ES cells to various hormones, including estrogen, may have affected the growth of ES cells.[14–16] Parp-1 has been suggested to be one of the key coactivator of estrogen receptor α-dependent transcriptional regulation, suggesting a possibility that the defective transduction of estrogen signaling in *Parp-1*$^{-/-}$ ES cells[17] may have attenuated growth of ES cells.

The reduced growth of the tumors derived from *Parp-1*$^{-/-}$ ES cells may also be related to the presence of induced trophoblasts. Trophoblast induction may have attenuated the growth of ES cell or the derived tumor cells more easily in the uterine environment compared to subcutaneous environment. After grafting of ES cells into the horn of the uterus, the ES cells seemed to become disseminated into the surrounding tissues and stroma. However, tumors did not develop in the lumen of the uterus.

Trophoblast giant cells were induced in the tumors derived from *Parp-1*$^{-/-}$ ES cells, but not in those from *Parp-1*$^{+/+}$ ES cells, similar to the case of teratocarcinoma development after subcutaneous grafting of these cells.[10] The TGCs were found in the tumors derived from *Parp-1*$^{-/-}$ ES cells as clusters in teratocarcinomas, suggesting that they were induced during teratocarcinoma formation after injection of the cells. Trophoblasts are known to express vasoregulatory factors, including inducible nitric oxide synthase, endothelial nitric oxide synthase,[18] adrenomedullin,[19] proliferin,[20] immunosuppressive factors, and proteases. Therefore, it is suggested that trophoblasts could be involved in metastasis under certain conditions. Notably, we observed metastastic lesions of the tumors in the liver and lung with *Parp-1*$^{-/-}$ ES cells. The frequency of invasion was also higher for *Parp-1*$^{-/-}$ cells than for *Parp-1*$^{+/+}$ cells. Although TGCs were not detected in the disseminated or invaded regions, there may be a possibility that trophoblast induction would be related to increased metastasis and invasion as described above. To examine whether TGCs and other trophoblasts are colocalized in the metastatic regions, it may be necessary to observe the tumor formation for a longer period. Another possible explanation for the increased frequencies of metastatic and invasive lesions under *Parp-1* deficiency could be that *Parp-1* deficiency may have increased the numbers of cancerous stem cells, which possess malignant phenotypes, through higher genomic instability that may enhance development of cancerous stem cells from ES cells in stressed conditions.[21] It may be also possible that *Parp-1* deficiency leads to resistance to a certain type of necrotic cell death, including reactive oxygen-induced cell death, which involves NAD depletion and Parp-1-dependent apoptosis-inducing factor activation.[22] This property may have promoted the survival of metastasizing *Parp-1*$^{-/-}$ ES cells.

In the present study, *Parp-1* deficiency was suggested to induce invasion and metastatic lesions of tumors that developed from ES cells in the uterus, which could not have been observed in our subcutaneous grafting model of ES cells.[10] The induction model of trophoblasts from *Parp-1*$^{-/-}$ ES cells during teratocarcinoma formation in the uterus and ovary environments may serve as a good model for elucidating the induction mechanism of trophoblast lineage differentiation and the role of trophoblasts during tumor formation. Recently, Parp-1 inhibitors have been in clinical trials as cancer therapies. The present study suggests the possibility that Parp-1 inhibition in germ cell tumors may be associated with a risk for metastatic lesion development accompanying trophoblast induction.

ACKNOWLEDGMENTS

This work was supported in part by a Grant-in-Aid for Cancer Research and a Grant-in-Aid for the Third Term Comprehensive 10-year Strategy for Cancer Control, Cancer Prevention from the Ministry of Health and Welfare of Japan (10103833), by MEXT KAKENHI (13216109), and by JSPS KAKENHI (22300343, 24593020). This work was also supported in part by a Grant-in-Aid for Cancer Research from the Ministry of Health, Labour and Welfare Japan (19-9). We appreciate the suggestions provided by Tomoharu Osada, Toshio Imai, Hippo Yoshitaka, Hitoshi Nakagama, Takahiro Ochiya, and Takashi Sugimura. T.N. was a recipient of a Research Grant from the Sankyo Foundation of Life Science.

REFERENCES

1 Masutani M, Nakagama H, Sugimura T. Poly (ADP-ribosyl)ation in relation to cancer and autoimmune disease. *Cell Mol Life Sci* 2005; **62**: 769–83.
2 Schreiber V, Dantzer F, Ame JC, de Murcia G. Poly (ADP-ribose): Novel functions for an old molecule. *Nat Rev Mol Cell Biol* 2006; **7**: 517–28.
3 Masutani M, Suzuki H, Kamada N *et al.* Poly(ADP-ribose) polymerase gene disruption conferred mice resistant to streptozotocin-induced diabetes. *Proc Natl Acad Sci U S A* 1996; **96**: 2301–4.
4 Masutani M, Nakagama H, Sugimura T. Poly (ADP-ribose) and carcinogenesis. *Genes Chromosomes Cancer* 2003; **38**: 339–48.
5 Masutani M, Nozaki T, Nishiyama E *et al.* Function of poly(ADP-ribose) polymerase in response to DNA damage: Gene-disruption study in mice. *Mol Cell Biochem* 1999; **193**: 149–52.
6 Miwa M, Masutani M. PolyADP-ribosylation and cancer. *Cancer Sci* 2007; **98**: 1528–35.
7 Kim MY, Mauro S, Gévry N, Lis JT, Kraus WL. NAD$^+$-dependent modulation of chromatin structure and transcription by nucleosome binding properties of PARP-1. *Cell* 2004; **119**: 803–14.
8 Krishnakumar R, Gamble MJ, Frizzell KM, Berrocal JG, Kininis M, Kraus WL. Reciprocal binding of PARP-1 and histone H1 at promoters specifies transcriptional outcomes. *Science* 2008; **319**: 819–21.
9 Wacker DA, Ruhl DD, Balagamwala EH, Hope KM, Zhang T, Kraus WL. The DNA binding and catalytic domains of poly(ADP-ribose) polymerase 1 cooperate in the regulation of chromatin structure and transcription. *Mol Cell Biol* 2007; **27**: 7475–85.
10 Nozaki T, Masutani M, Watanabe M *et al.* Syncytiotrophoblastic giant cells in teratocarcinoma-like tumors derived from Parp-disrupted mouse embryonic stem cells. *Proc Natl Acad Sci U S A* 1999; **96**: 13345–50.
11 Hemberger M, Nozaki T, Winterhager E *et al.* Parp1-deficiency induces differentiation of ES cells into trophoblast derivatives. *Dev Biol* 2003; **257**: 371–81.

12 Ogino H, Nozaki T, Gunji A. Loss of Parp-1 affects gene expression profile in a genome-wide manner in ES cells and liver cells. *BMC Genomics* 2007; **8**: 41.
13 Cross JC, Hemberger M, Lu Y *et al.* Trophoblast functions, angiogenesis and remodeling of the maternal vasculature in the placenta. *Mol Cell Endocrinol* 2002; **187**: 207–12.
14 Monzo M, de Anta JM, Peris B, Ruano D. Growth control of embryonic stem cells injected into mouse uterus on fifth day of pregnancy. *Int J Cancer* 1994; **56**: 387–92.
15 Ogawa K, Matsui H, Ohtsuka S, Niwa H. A novel mechanism for regulating clonal propagation of mouse ES cells. *Genes Cells* 2004; **9**: 471–7.
16 Díaz NF, Díaz-Martínez NE, Camacho-Arroyo I, Velasco I. Estradiol promotes proliferation of dopaminergic precursors resulting in a higher proportion of dopamine neurons derived from mouse embryonic stem cells. *Int J Dev Neurosci* 2009; **27**: 493–500.
17 Zhang F, Wang Y, Wang L *et al.* Poly (ADP-ribose) polymerase 1 is a key regulator of estrogen receptor α-dependent gene transcription. *J Biol Chem* 2013; **288**: 11348–57.
18 Gagioti S, Scavone C, Bevilacqua E. Participation of the mouse implanting trophoblast in nitric oxide production during pregnancy. *Biol Reprod* 2000; **62**: 260–68.
19 Yotsumoto S, Shimada T, Cui CY, Nakashima H, Fujiwara H, Ko MS. Expression of adrenomedullin, a hypotensive peptide, in the trophoblast giant cells at the embryo implantation site in mouse. *Dev Biol* 1998; **203**: 264–75.
20 Jackson D, Volpert OV, Bouck N, Linzer DI. Stimulation and inhibition of angiogenesis by placental proliferin and proliferin-related protein. *Science* 1994; **266**: 1581–4.
21 Fujimori H, Shikanai M, Teraoka H, Masutani M, Yoshioka K. Induction of cancerous stem cells during embryonic stem cell differentiation. *J Biol Chem* 2012; **26**: 36777–91.
22 Yu SW, Andrabi SA, Wang H *et al.* Apoptosis-inducing factor mediates poly(ADP-ribose) (PAR) polymer-induced cell death. *Proc Natl Acad Sci U S A* 2006; 28: **103**: 18314–19.

Molecular Aspects of Medicine 34 (2013) 1202–1216

Contents lists available at SciVerse ScienceDirect

Molecular Aspects of Medicine

journal homepage: www.elsevier.com/locate/mam

Review

Poly(ADP-ribosyl)ation in carcinogenesis

Mitsuko Masutani *, Hiroaki Fujimori

Division of Genome Stability Research, National Cancer Center Research Institute, Japan

ARTICLE INFO

Article history:
Available online 25 May 2013

ABSTRACT

Cancer develops through diverse genetic, epigenetic and other changes, so-called 'multi-step carcinogenesis', and each cancer harbors different alterations and properties. Here in this article we review how poly(ADP-ribosyl)ation is involved in multi-step and diverse pathways of carcinogenesis. Involvement of poly- and mono-ADP-ribosylation in carcinogenesis has been studied at molecular and cellular levels, and further by animal models and human genetic approaches. PolyADP-ribosylation acts in DNA damage repair response and maintenance mechanisms of genomic stability. Several DNA repair pathways, including base-excision repair and double strand break repair pathways, involve PARP and PARG functions. These care-taker functions of poly(ADP-ribosyl)ation suggest that polyADP-ribosylation may mainly act in a tumor suppressive manner because genomic instability caused by defective DNA repair response could serve as a driving force for tumor progression, leading to invasion, metastasis and relapse of cancer. On the other hand, the new concept of 'synthetic lethality by PARP inhibition' suggests the significance of PARP activities for survival of cancer cells that harbor defects in DNA repair. Accumulating evidence has revealed that some PARP family molecules are involved in various signaling cascades other than DNA repair, including epigenetic and transcriptional regulations, inflammation/immune response and epithelial-mesenchymal transition, suggesting that poly(ADP-ribosyl)ation both promotes and suppresses carcinogenic processes depending on the conditions.

Expanding understanding of poly(ADP-ribosyl)ation suggests that strategies to achieve cancer prevention targeting poly(ADP-ribosyl)ation for genome protection against life-long exposure to environmental carcinogens and endogenous carcinogenic stimuli.

Contents

* Corresponding author. Address: Division of Genome Stability Research, National Cancer Center Research Institute, 5-1-1 Tsukiji, Chuo-ku, Tokyo 104-0045, Japan. Tel.: +81 3 3547 5201x4350; fax: +81 3 3543 9305.
E-mail address: mmasutan@ncc.go.jp (M. Masutani).

0098-2997/$ - see front matter © 2013 Elsevier Ltd. All rights reserved.
http://dx.doi.org/10.1016/j.mam.2013.05.003